HIBERNATION

Suppression of neurons in circumventricular organs enables months-long survival without water in thirteen-lined ground squirrels

Madeleine S. Junkins[1,2,3], Ni Y. Feng[1,2,3]†, Dana K. Merriman[4], Sviatoslav N. Bagriantsev[1]*, Elena O. Gracheva[1,2,3,5]*

Water deprivation is a life-threatening condition that engages a protective physiological response to couple osmolyte retention with potentiation of thirst. This response, typical for most mammals, safeguards against short-term water deprivation but fails in the long term. Thirteen-lined ground squirrels (*Ictidomys tridecemlineatus*) use the short-term response during summer, whereas during winter, they lack thirst and survive without water for months. In this work, we show that long-term thirst suppression occurs despite hormonal and behavioral signs of a substantial fluid deficit and originates from hypoactivity of neurons in the circumventricular organs, which exhibit marked functional suppression during winter that blunts their sensitivity to thirst cues. Our work reveals a notable capacity of the evolutionarily conserved brain regions that control fluid homeostasis in mammals to enable long-term survival without water.

Thirst is a powerful drive that results from fluid imbalance and promotes drinking when water becomes available (*1*–*5*). However, water access varies widely depending on species' habitats. Whereas humans cannot survive without water for long, desert natives such as kangaroo rats never drink at all (*6*). Nevertheless, all mammals rely on a similar neuroendocrine pathway to stay hydrated (*7*, *8*), suggesting that the principles of fluid homeostasis may be better understood by considering extreme cases (*9*).

The thirteen-lined ground squirrel (*Ictidomys tridecemlineatus*) hibernates for 6 to 8 months without water (*10*–*12*). In winter, hibernating squirrels remain within their burrows, cycling between two physiological states: torpor and interbout arousal (*11*). Torpor is a period of inactivity and suppressed metabolism, during which body temperature approaches 2° to 4°C. Torpor bouts last 2 to 3 weeks and are punctuated by spontaneous ~24- to 48-hour interbout arousals. A squirrel in interbout arousal achieves a core body temperature of 37°C and will move around in its burrow but does not leave in search of water (*10*, *13*) and refuses to drink when given the opportunity (*10*, *12*). The neurophysiological mechanism by which hibernators survive for months without drinking is a question that has gone unanswered, despite more than a century's worth of hibernation research (*14*).

In all mammals, the renal and nervous systems cooperate to maintain fluid homeostasis (*2*). Water deprivation can lead to hyperosmolality, hypotension, and/or hypovolemia (*7*, *15*), all of which trigger the production of angiotensin II and aldosterone (*2*, *16*). In the kidneys, angiotensin II potentiates sodium and water reabsorption in the proximal tubules, whereas aldosterone up-regulates the reabsorption of sodium in the distal tubules, indirectly promoting water retention (*2*, *17*). These hormones also act in the central nervous system: Aldosterone activates hindbrain neurons to generate an appetite for sodium, whereas angiotensin II prompts the release of antidiuretic hormone from the posterior pituitary and promotes drinking (*16*, *18*, *19*).

Neural regulation of fluid homeostasis is attributed to a set of subcortical nuclei that sense and respond to dehydration (*7*, *8*). Elevated serum angiotensin II and osmolality are sensed by neurons in the subfornical organ (SFO) and organum vasculosum laminae terminalis (OVLT), which reside outside of the blood-brain barrier (*20*, *21*). SFO and OVLT neurons project to distinct hypothalamic regions that stimulate the release of vasopressin and oxytocin into circulation (*22*) and promote thirst (*4*, *23*). In this work, we hypothesized that thirst is inhibited during hibernation by a neuronal mechanism that originates in the SFO and OVLT.

Hibernating squirrels show signs of fluid deficiency

We set out to elucidate the hydration status of the hibernator, focusing on squirrels in interbout arousal because they resemble active animals in terms of cardiovascular function, body temperature, and activity (*11*) but lack thirst. We reported that squirrels in interbout arousal show blood levels of osmolality, vasopressin, and oxytocin that are comparable to those of active squirrels, despite spending months without water (*10*, *12*). These findings indicate that squirrels are not hyperosmotic during hibernation; however, we speculated that other signs of fluid deficiency might exist. Indeed, we found that serum angiotensin II doubled and aldosterone nearly tripled during hibernation (Fig. 1, A and B). We previously found that serum blood urea nitrogen levels drop during hibernation, suggesting that angiotensin II and aldosterone elevation do not result from kidney stress (*10*). Sometimes elevated aldosterone is associated with hyperkalemia (*17*); however, we previously reported that there is no difference in serum potassium levels between active and interbout arousal squirrels (*10*).

Ruling out kidney stress and hyperkalemia, it is likely that high angiotensin II and aldosterone levels result from a reduction in body fluid volume during hibernation. This could take the form of hypovolemia and/or hypotension, both of which are known to stimulate a robust sodium appetite in addition to thirst (*15*, *18*, *24*, *25*). Indeed, we found that squirrels in interbout arousal exhibited an appetite for 0.5 M NaCl, which active squirrels avoided (Fig. 1, C to E). Interbout arousal squirrels drank more 0.5 M NaCl than water (Fig. 1E), and this phenomenon did not extend to 0.5 M KCl (Fig. 1F). These results indicate that interbout arousal squirrels are fluid deficient and sensitive to circulating cues for sodium appetite (aldosterone), but they have a blunted sensitivity to thirst cues (angiotensin II, blood osmolality).

We previously recorded drops in blood osmolality, potassium, vasopressin, and oxytocin during torpor, which suggests that torpor physiology differs from interbout arousal (*10*, *12*). In this work, we found that torpid squirrels also showed much lower serum angiotensin II and aldosterone than squirrels in interbout arousal (fig. S1). These data suggest that fluid deficiency is specifically sensed during interbout arousal, when vital signs and activity recover to active levels.

Squirrels do not have access to food or water during hibernation. Because starvation is reported to suppress thirst in some species (*26*), we tested whether fasting could suppress thirst in active squirrels. We found that fasting did not affect thirst (Fig. 1, G and H), which suggests that lack of food alone is unlikely to cause thirst suppression during interbout arousal.

Thirst neurons from hibernating squirrels retain angiotensin II sensitivity

To explore potential neural mechanisms for thirst suppression, we turned to SFO and OVLT

[1]Department of Cellular and Molecular Physiology, Yale University School of Medicine, New Haven, CT, USA. [2]Department of Neuroscience, Yale University School of Medicine, New Haven, CT, USA. [3]Department of Neuroscience and Program in Cellular Neuroscience, Neurodegeneration and Repair, Yale University School of Medicine, New Haven, CT, USA. [4]Department of Biology, University of Wisconsin–Oshkosh, Oshkosh, WI, USA. [5]Kavli Institute for Neuroscience, Yale University School of Medicine, New Haven, CT, USA.
*Corresponding author. Email: slav.bagriantsev@yale.edu (S.N.B.); elena.gracheva@yale.edu (E.O.G.)
†Present address: Department of Biology, Wesleyan University, Middletown, CT, USA.

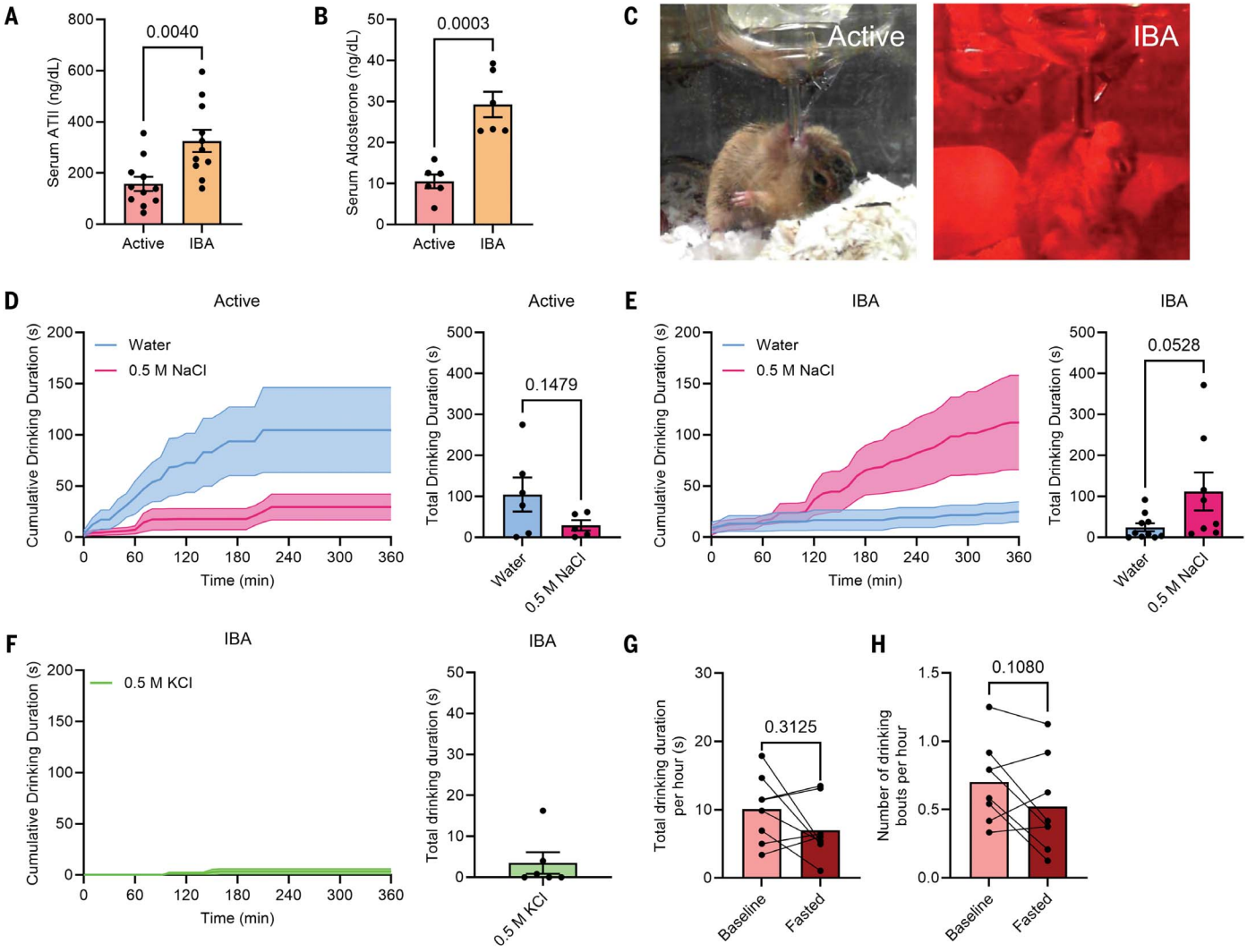

Fig. 1. Hibernating squirrels exhibit thirst suppression despite signs of fluid deficiency. (**A**) Serum angiotensin II measurements from active (n = 11) and interbout arousal (n = 11) squirrels. Data were analyzed by unpaired t test. (**B**) Serum aldosterone measurements from active (n = 6) and interbout arousal (n = 6) squirrels. Data were analyzed by unpaired t test. (**C**) Representative images of active (left) and interbout arousal (right) squirrels drinking. Interbout arousal drinking behavior is recorded under red light. (**D**) Cumulative time spent drinking water (blue) or 0.5 M NaCl (pink) for active squirrels shown as mean ± SE (left) and quantification of time spent drinking water (n = 6) or 0.5 M NaCl (n = 5) (right) over 6 hours. Data were analyzed by unpaired t test. (**E**) Cumulative time spent drinking water (blue) or 0.5 M NaCl (pink) for interbout arousal squirrels ($n \geq 8$) shown as mean ± SE (left) and quantification of time spent drinking water (n = 10) or 0.5 M NaCl (n = 8) (right) over 6 hours. Data were analyzed by Mann-Whitney test. (**F**) Cumulative time spent drinking 0.5 M KCl (green) for interbout arousal squirrels shown as mean ± SE (left) and quantification of time spent drinking 0.5 M KCl (n = 6) (right) over 6 hours. (**G**) Total drinking duration per hour for active squirrels (n = 8) at baseline and during 48 hours of food deprivation. Data were analyzed by Wilcoxon matched-pairs signed rank test. (**H**) Number of drinking bouts per hour for active squirrels (n = 8) at baseline and during 48 hours of food deprivation. Data were analyzed by paired t test. Dots represent data from individual animals (mean ± SE). The numbers above the data brackets denote p values. ATII, angiotensin II; IBA, interbout arousal.

neurons, which sense elevated levels of circulating angiotensin II and drive thirst (*2*, *7*, *8*). We found that the levels of angiotensin II receptor 1 *Agtr1* remain unchanged in the SFO during interbout arousal (Fig. 2, A and B). To test whether angiotensin II can reach thirst neurons during hibernation, we injected fluorescently labeled angiotensin II intra-arterially and measured fluorescence intensity. We did not observe differences in angiotensin II binding between active and interbout arousal animals in the SFO (Fig. 2, C and D, and fig. S2A) or OVLT (Fig. 2, E and F, and fig. S2B). To test whether thirst neurons can respond to angiotensin II during hibernation, we dissociated SFO and OVLT neurons and performed calcium imaging (Fig. 2, G and K). We found that angiotensin II triggered robust responses in both populations and both states; indeed, there was an increase in peak angiotensin II response in OVLT neurons during interbout arousal (Fig. 2L). We also observed an increase in the proportion of responders from interbout arousal neurons compared with active neurons in the SFO and OVLT (Fig. 2, I and M). These results demonstrate that interbout arousal thirst neurons can sense and respond to angiotensin II. Thus, the mechanism for thirst suppression is likely independent from angiotensin II signaling in the SFO and OVLT.

We also observed that peak responses to high K^+ application were significantly lower in SFO and OVLT neurons from squirrels in

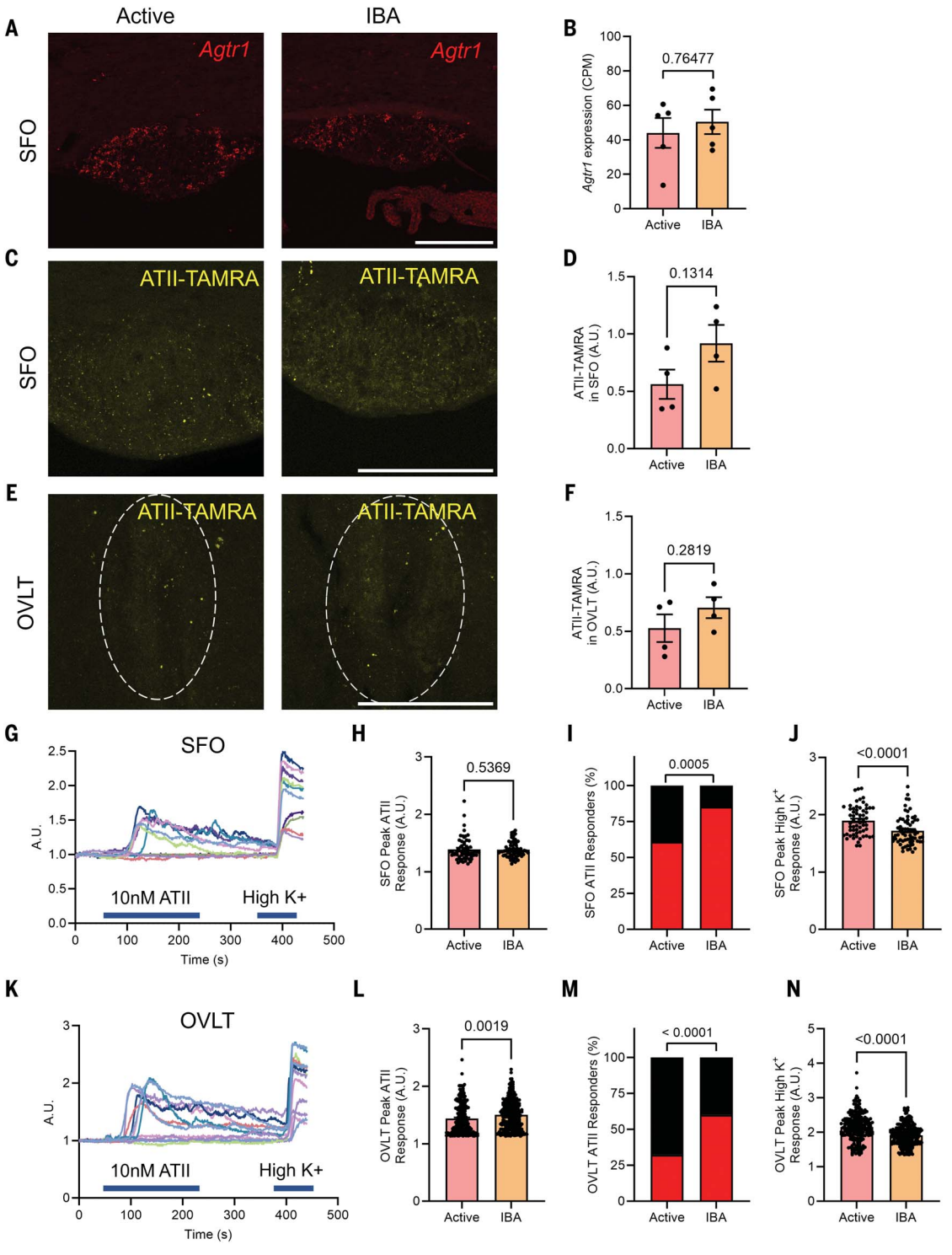

Fig. 2. Thirst neurons in the SFO and OVLT can respond to angiotensin II during hibernation. (**A**) RNAScope images of SFO from active and interbout arousal squirrels probed for *Agtr1*. (**B**) Quantification of *Agtr1* transcripts in SFO from active (n = 5) and interbout arousal (n = 5) squirrels. Dots represent data from individual animals (mean ± SE). Data were analyzed by generalized linear model. (**C**) Representative confocal images of SFO from active and interbout arousal squirrels injected intra-arterially with angiotensin II bound to the fluorescent dye TAMRA (ATII-TAMRA) (yellow). (**D**) Quantification of ATII-TAMRA dye intensity in SFO from active (n = 4) and interbout arousal (n = 4) squirrels normalized to liver intensity. Dots represent an average of three or more images from individual animals (mean ± SE). Data were analyzed by unpaired t test. (**E**) Representative confocal images of OVLT from active and interbout arousal squirrels injected intra-arterially with ATII-TAMRA (yellow). White dashed ovals indicate the borders of the OVLT. (**F**) Quantification of ATII-TAMRA dye intensity in OVLT from active (n = 4) and interbout arousal (n = 4) squirrels normalized to liver intensity. Dots represent an average of three or more images from individual animals (mean ± SE). Data were analyzed by unpaired t test. (**G**) Representative traces from ratiometric calcium imaging of dissociated SFO neurons. Traces show fluorescence during bath application of angiotensin II followed by high K^+. (**H**) Peak responses to angiotensin II from active (n = 60 neurons from six squirrels) and interbout arousal (n = 66 neurons from 11 squirrels) SFO neurons. Data were analyzed by Mann-Whitney test. (**I**) Proportions of active and interbout arousal SFO neurons that responded to angiotensin II (red) or did not (black). Data were analyzed by chi-square test. (**J**) Peak responses to high K^+ from active (n = 60 neurons from six squirrels) and interbout arousal (n = 66 neurons from 11 squirrels) angiotensin II–responsive SFO neurons. Data were analyzed by Mann-Whitney test. (**K**) Representative traces from ratiometric calcium imaging of dissociated OVLT neurons. Traces show fluorescence during bath application of angiotensin II followed by high K^+. (**L**) Peak responses to angiotensin II from active (n = 227 neurons from four squirrels) and interbout arousal (n = 282 neurons from four squirrels) OVLT neurons. Data were analyzed by Mann-Whitney test. (**M**) Proportions of active and interbout arousal OVLT neurons that responded to angiotensin II (red) or did not (black). Data were analyzed by chi-square test. (**N**) Peak responses to high K^+ from active (n = 227 neurons from four squirrels) and IBA (n = 282 neurons from four squirrels) angiotensin II–responsive OVLT neurons. Data were analyzed by Mann-Whitney test. Unless otherwise indicated, dots represent individual neurons (mean ± SE). The numbers above the data brackets denote p values. Scale bars are 200 μm. ATII, angiotensin II; A.U., arbitrary units (of fluorescence); IBA, interbout arousal.

interbout arousal (Fig. 2, J and N). These data suggest that interbout arousal neurons are able to sense angiotensin II but may be impaired in other ways.

Thirst neuron activity is suppressed during hibernation

We next asked whether thirst suppression arises from reduced baseline activity of thirst neurons. Using c-FOS as a proxy for neuronal activity, we determined a reduction in total activity in the SFO and OVLT during interbout arousal (Fig. 3, A, B, E, and F). This reduction was due in part to $nNOS^+$ excitatory neurons and $nNOS^-$ neurons, most of which are likely to be inhibitory (Fig. 3, C, D, G, and H, and fig. S3) (*15*). Next, we tested whether thirst neurons would also have a blunted response to osmotic challenge by injecting active and interbout arousal squirrels with 3 M NaCl and assessing changes in serum osmolality and $c\text{-}FOS^+$ neuron number. Although 3 M NaCl treatment produced identically high serum osmolality in both states (fig. S4) (*10*), it elicited fewer $c\text{-}FOS^+$ $nNOS^+$ SFO neurons in interbout arousal than in the active state (Fig. 3, J and K), and we observed a similar trend with $c\text{-}FOS^+$ $nNOS^+$ OVLT neurons (Fig. 3O). These results reveal that in the OVLT and SFO, which are the earliest points in the neural pathway for fluid homeostasis, thirst neurons have suppressed baseline and osmosensory activity during interbout arousal.

SFO neurons are hypoactive and more sensitive to GABA during hibernation

We next hypothesized that SFO neurons would exhibit reduced intrinsic excitability, consistent with the global reduction in $c\text{-}FOS^+$ neuron number. To test this, we performed electrophysiological recordings with dissociated SFO neurons from both states (Fig. 4A). Active neurons exhibited basic electrophysiological properties similar to those reported from SFO neurons in other species (*27*, *28*), whereas interbout arousal neurons were comparatively hypoactive (Fig. 4, B and C). Although neurons from both states were the same size (Fig. 4D), interbout arousal neurons had significantly higher input resistance, suggesting a decrease in leak conductances (Fig. 4E). Although high input resistance may potentiate excitability in some cases (*29*), we found that interbout arousal neurons were hyperpolarized (Fig. 4F) and silent compared with active neurons (Fig. 4G).

A 3- to 10-pA current injection triggered firing in interbout arousal neurons and revealed differences in action potential waveforms between states (Fig. 4H): Interbout arousal neurons took longer to reach peak amplitude, and the average peak was smaller in amplitude compared with that of active neurons (Fig. 4, I and J). The same was true for the time to maximal hyperpolarization, whereas the maximal hyperpolarization amplitude was more negative in interbout arousal neurons (Fig. 4, K and L). Interbout arousal neurons also exhibited a shallower rise slope, longer rise time, and larger half-width than active neurons (Fig. 4, M to O). These results indicate that interbout arousal neurons are functionally impaired compared with active neurons.

We found an apparent increase in expression of the type A γ-aminobutyric acid ($GABA_A$) receptor transcript *Gabrg1* in interbout arousal SFO (Fig. 4P), suggesting that neurons may be more potently inhibited by GABA during hibernation. To test this, we compared GABA's effect on firing rate while applying a small amount of holding current so that interbout arousal neurons would fire spontaneously. Ten micromolar GABA reduced firing frequency to near zero in both states. However, whereas active neurons recovered their initial firing frequency upon washout (Fig. 4Q), interbout arousal neurons remained suppressed after GABA removal (Fig. 4Q). These results demonstrate that interbout arousal SFO neurons are much slower to recover from GABA inhibition.

Discussion

Thirst is an interoceptive sensation that follows from water deprivation and/or fluid loss (*7*). Although we conceive of thirst as being indispensable for survival, this is not always the case; for species living in water-scarce environments, thirst is not a relevant signal. Desert rodents forgo drinking altogether: Pack rats consume water-rich plants instead, and kangaroo rats subsist on dry food (*6*). By contrast, thirteen-lined ground squirrels eat and drink freely in the warmer months but avoid food and water during hibernation (*9*–*12*, *30*).

In species that drink regularly, water deprivation results in a combination of hyperosmolality and hypovolemia (*7*). However, this is not the case for hibernating squirrels; we previously found that serum osmolality never overshoots the set point for active squirrels (*10*). Instead, hibernating squirrels appear to experience a contraction in blood volume that results from respiration and the production of concentrated urine, which is known to occur during interbout arousal (*31*). Consistent with this, we found that angiotensin II and aldosterone are elevated during interbout arousal in hibernating squirrels compared with active squirrels (Fig. 1, A and B), suggesting that squirrels are hypovolemic but not hyperosmotic.

Hypovolemia drives nonhibernating rodents to ingest water and aversive concentrations of saline indiscriminately because both can restore blood volume (*2*, *7*, *15*). Although no previous studies have reported an appetite for sodium in the absence of thirst, as is seen in interbout arousal (Fig. 1E), it may theoretically become possible when an animal is so hypovolemic that ingesting pure water could interfere with circulating levels of critical osmolytes (*32*, *33*).

Whether this is the case in interbout arousal remains to be established, but there is another, nonmutually exclusive possibility: Neurons that control sodium appetite (*16*, *25*) remain functional, whereas thirst neurons are suppressed. We found that baseline activity in thirst neurons is substantially reduced during hibernation (Fig. 4, B to G). Further, when challenged with acute hyperosmolality, fewer neurons are activated during hibernation (Fig. 3, I to P). Lastly, inhibition of interbout arousal thirst neurons with GABA results in prolonged silence compared with inhibition of active neurons (Fig. 4Q). Although neuronal dissociation removes external sources of excitation and inhibition, active and interbout arousal squirrels are comparable in terms of body temperature and serum osmolality, so it is likely that our electrophysiological data reveal true cell-intrinsic differences in thirst neuron function across states. Together, our results indicate that thirst neurons are suppressed during hibernation, which enables the silencing of thirst.

Importantly, it is unlikely that neurons throughout the entire brain are unilaterally suppressed throughout hibernation. Studies from several hibernating species suggest that the activity of distinct neural populations is differentially regulated across torpor and interbout arousal, depending on physiological need (*30*, *34*–*38*). In the future, it will be essential to explore how different neural circuits that regulate homeostatic functions are suppressed or spared.

Surprisingly, the neural mechanism for thirst suppression appears to be independent from the angiotensin II signaling pathway. Thirst neurons clearly possess the ability to detect and respond to angiotensin II throughout hibernation (Fig. 2, A to F). Angiotensin II is known to depolarize dissociated SFO neurons, which may explain why even hypoactive interbout arousal neurons respond to angiotensin II (Fig. 2, H and L) (*27*). It was reported that SFO neurons from mice that lack *Tmem63b* lose sensitivity to osmotic stimuli while retaining the ability to respond to angiotensin II (*28*), adding to the body of work supporting the idea that osmotic and hormonal stimuli are separable within thirst neurons (*20*, *39*, *40*). Recent reports have revealed that distinct thirst neuron subpopulations are recruited during water deprivation, sodium depletion, and hypovolemia (*15*, *25*, *41*). Together, this body of work indicates that thirst neurons are able to distinguish between numerous challenges to fluid homeostasis. We found that $c\text{-}FOS^+$ neuron number is reduced during interbout arousal (Fig. 3), despite high serum angiotensin II, which indicates that the ability to sense angiotensin II is insufficient to stimulate neuronal activity and thirst in vivo during hibernation. We also found that dissociated thirst neurons show

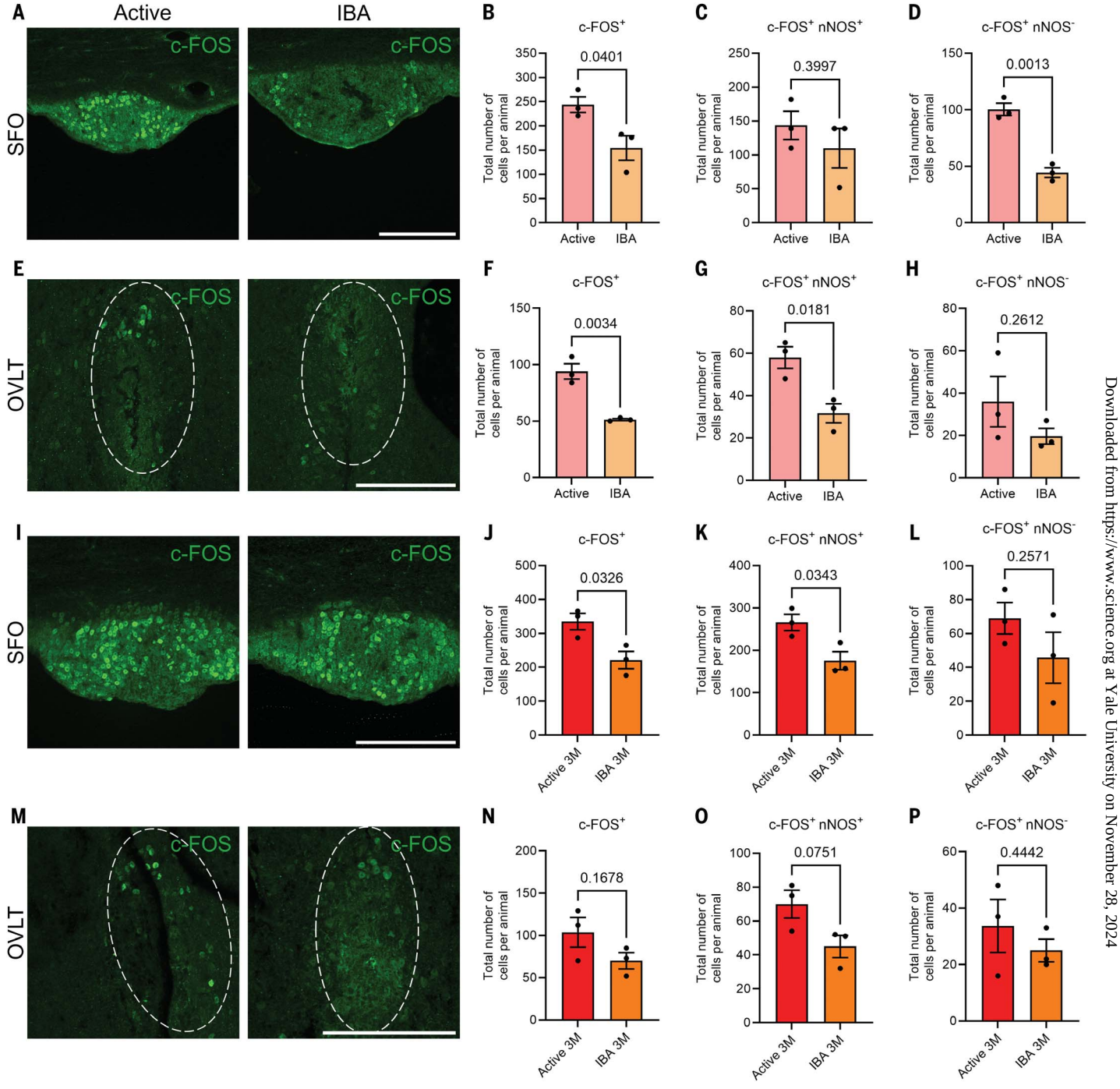

Fig. 3. Thirst neuron activity is suppressed during hibernation.
(**A**) Representative immunohistochemical images showing c-FOS$^+$ (green) cells in the SFO from active and interbout arousal squirrels. (**B** to **D**) Total number of c-FOS$^+$ SFO neurons (B), total number of c-FOS$^+$ nNOS$^+$ SFO neurons (C), and total number of c-FOS$^+$ nNOS$^-$ SFO neurons (D) from active and interbout arousal squirrels. (**E**) Representative immunohistochemical images showing c-FOS$^+$ (green) cells in the OVLT from active and interbout arousal squirrels. White dashed ovals indicate the borders of the OVLT. (**F** to **H**) Total number of c-FOS$^+$ OVLT neurons (F), total number of c-FOS$^+$ nNOS$^+$ OVLT neurons (G), and total number of c-FOS$^+$ nNOS$^-$ OVLT neurons (H) from active and interbout arousal squirrels. (**I**) Representative immunohistochemical images showing c-FOS$^+$ (green) cells in the SFO from active and interbout arousal squirrels treated with 3 M NaCl intraperitoneally (i.p.). (**J** to **L**) Total number of c-FOS$^+$ SFO neurons (J), total number of c-FOS$^+$ nNOS$^+$ SFO neurons (K), and total number of c-FOS$^+$ nNOS$^-$ SFO neurons (L) from active and interbout arousal squirrels treated with 3 M NaCl i.p. (**M**) Representative immunohistochemical images showing c-FOS$^+$ (green) cells in the OVLT from active and interbout arousal squirrels treated with 3 M NaCl i.p. White dashed ovals indicate the borders of the OVLT. (**N** to **P**) Total number of c-FOS$^+$ OVLT neurons (N), total number of c-FOS$^+$ nNOS$^+$ OVLT neurons (O), and total number of c-FOS$^+$ nNOS$^-$ OVLT neurons (P) from active and interbout arousal squirrels treated with 3 M NaCl i.p. Dots represent data from three individual animals (mean ± SE). The numbers above the data brackets denote p values from an unpaired t test. Scale bars are 200 μm. IBA, interbout arousal.

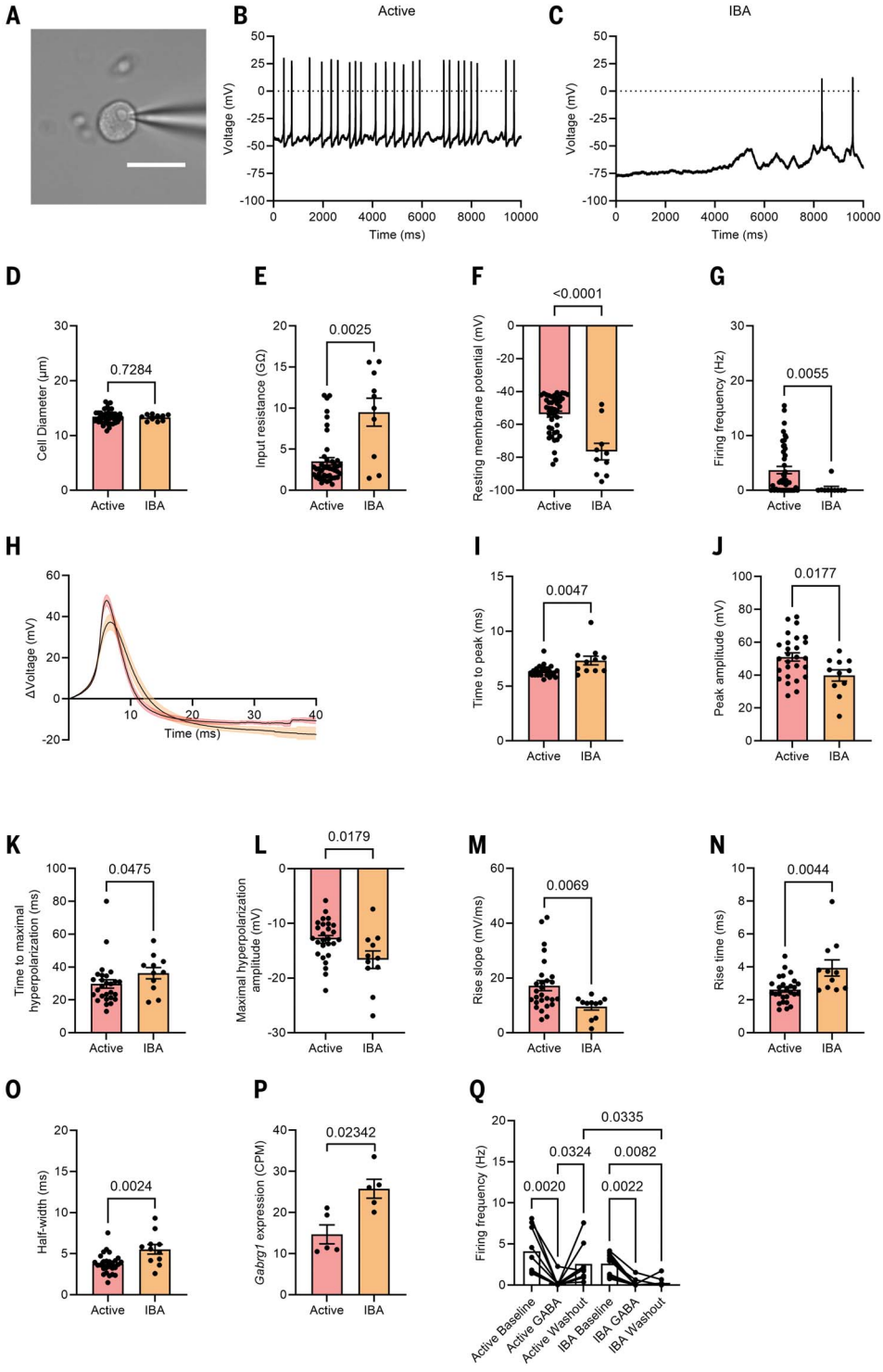

Fig. 4. Electrophysiological activity of SFO neurons is suppressed during hibernation. (**A**) Representative bright-field microscopy image of a dissociated SFO neuron undergoing patch-clamp electrophysiological recording. Scale bar is 20 µm. (**B**) Representative trace of an active SFO neuron in a current clamp. (**C**) Representative trace of an interbout arousal SFO neuron in a current clamp. (**D**) Diameter of active (n = 41 neurons from 10 squirrels) and interbout arousal (n = 10 neurons from six squirrels) SFO neurons. Data were analyzed by unpaired t test. (**E**) Input resistance of active (n = 43 neurons from 10 squirrels) and interbout arousal (n = 10 neurons from six squirrels) SFO neurons. Data were analyzed by Mann-Whitney test. (**F**) Resting membrane potential of active (n = 44 neurons from 10 squirrels) and interbout arousal (n = 10 neurons from six squirrels) SFO neurons. Data were analyzed by Mann-Whitney test. (**G**) Firing frequency at rest of active (n = 44 neurons from 10 squirrels) and interbout arousal (n = 10 neurons from six squirrels) SFO neurons. Data were analyzed by Mann-Whitney test. (**H**) Active (pink) and interbout arousal (orange) AP waveforms, normalized to the baseline at the start of the event and shown as mean ± SE. For (H) to (O) and (Q), interbout arousal neurons were held to a current between 3 and 10 pA to induce baseline firing. (**I**) AP time to peak of active (n = 27 neurons from 10 squirrels) and interbout arousal (n = 11 neurons from six squirrels) SFO neurons. Data were analyzed by Mann-Whitney test. (**J**) AP peak amplitude of active (n = 27 neurons from 10 squirrels) and interbout arousal (n = 11 neurons from six squirrels) SFO neurons. Data were analyzed by unpaired t test. (**K**) AP time to maximal hyperpolarization of active (n = 27 neurons from 10 squirrels) and interbout arousal (n = 11 neurons from six squirrels) SFO neurons. Data were analyzed by Mann-Whitney test. (**L**) AP maximal hyperpolarization amplitude of active (n = 27 neurons from 10 squirrels) and interbout arousal (n = 11 neurons from six squirrels) SFO neurons. Data were analyzed by unpaired t test. (**M**) AP rise slope of active (n = 27 neurons from 10 squirrels) and interbout arousal (n = 11 neurons from six squirrels) SFO neurons. Data were analyzed by Mann-Whitney test. (**N**) AP rise time of active (n = 27 neurons from 10 squirrels) and interbout arousal (n = 11 neurons from six squirrels) SFO neurons. Data were analyzed by Mann-Whitney test. (**O**) AP half-width of active (n = 27 neurons from 10 squirrels) and interbout arousal (n = 11 neurons from six squirrels) SFO neurons. Data were analyzed by Mann-Whitney test. (**P**) Quantification of *Gabrg1* transcripts in SFO from active (n = 5) and interbout arousal (n = 5) squirrels. CPM, counts per million. Dots represent individual animals (mean ± SE). Data were analyzed by generalized linear model; false discovery ratio (FDR) = 0.232. (**Q**) AP frequency before, during, and after bath application of GABA in active and interbout arousal neurons. Data were analyzed by Kruskal-Wallis test with multiple comparisons. Unless otherwise indicated, dots represent neurons (mean ± SE). The numbers above the data brackets denote p values. AP, action potential; IBA, interbout arousal.

prolonged inhibition by GABA, raising the possibility that, in the presence of GABA-releasing inputs from other regions, interbout arousal neurons are too inhibited to respond to angiotensin II. In vivo experiments are required to identify the molecular and circuit-level changes that underlie the notable silencing of thirst neurons during interbout arousal and to establish the causality of these changes in suppressing

thirst. One limitation of our study is the minimal cell-type specificity that experiments in our nonmodel system can provide. Recent work has revealed the extent of thirst neurons' heterogeneity (*15*, *25*), and it is likely that different subpopulations perform specific roles that have yet to be revealed in the context of hibernation.

How do hibernators survive the winter without water or thirst? We propose that squirrels use a two-pronged strategy to optimize water conservation while minimizing thirst. We previously reported that antidiuretic hormone–releasing neurons of the supraoptic nucleus become activated below 10°C in vivo to promote water retention during the transition from torpor to interbout arousal (*12*). By releasing antidiuretic hormones early during arousal, squirrels may retain at least some body water that would otherwise be lost to diuresis (*12*). In this work, we show that, when the transition to interbout arousal is complete, squirrels remain insensitive to physiological cues for thirst. Our work elucidates the neurophysiological adaptations to the fluid homeostasis pathway that underlie the hibernator's notable ability to remain in a state of suspended animation within the burrow and without water.

REFERENCES AND NOTES

1. W. E. Allen *et al*., *Science* **357**, 1149–1155 (2017).
2. J. T. Fitzsimons, *Physiol. Rev.* **78**, 583–686 (1998).
3. Y. Oka, M. Ye, C. S. Zuker, *Nature* **520**, 349–352 (2015).
4. V. Augustine *et al*., *Nature* **555**, 204–209 (2018).
5. C. A. Zimmerman *et al*., *Nature* **537**, 680–684 (2016).
6. K. Schmidt-Nielsen, B. Schmidt-Nielsen, *Physiol. Rev.* **32**, 135–166 (1952).
7. D. E. Leib, C. A. Zimmerman, Z. A. Knight, *Curr. Biol.* **26**, R1260–R1265 (2016).
8. V. Augustine, S. Lee, Y. Oka, *Cell* **180**, 25–32 (2020).
9. M. S. Junkins, S. N. Bagriantsev, E. O. Gracheva, *J. Exp. Biol.* **225**, jeb229542 (2022).
10. N. Y. Feng, M. S. Junkins, D. K. Merriman, S. N. Bagriantsev, E. O. Gracheva, *Curr. Biol.* **29**, 3053–3058.e3 (2019).
11. S. M. Mohr, S. N. Bagriantsev, E. O. Gracheva, *Annu. Rev. Cell Dev. Biol.* **36**, 315–338 (2020).
12. M. S. Junkins *et al*., *Curr. Biol.* **34**, 923–930.e5 (2024).
13. B. Kisser, H. T. Goodwin, *Am. Midl. Nat.* **167**, 396–409 (2012).
14. A. T. Rasmussen, *Am. Nat.* **50**, 609–625 (1916).
15. A. H. Pool *et al*., *Nature* **588**, 112–117 (2020).
16. J. M. Resch *et al*., *Neuron* **96**, 190–206.e7 (2017).
17. A. Spät, L. Hunyady, *Physiol. Rev.* **84**, 489–539 (2004).
18. J. C. Geerling, A. D. Loewy, *Exp. Physiol.* **93**, 177–209 (2008).
19. B. C. Jarvie, R. D. Palmiter, *Nat. Neurosci.* **20**, 167–169 (2017).
20. A. I. Hicks, S. Kobrinsky, S. Zhou, J. Yang, M. Prager-Khoutorsky, *Front. Cell. Neurosci.* **15**, 691711 (2021).
21. M. Prager-Khoutorsky, C. W. Bourque, *Am. J. Physiol. Regul. Integr. Comp. Physiol.* **309**, R324–R337 (2015).
22. C. W. Bourque, *Nat. Rev. Neurosci.* **9**, 519–531 (2008).
23. D. E. Leib *et al*., *Neuron* **96**, 1272–1281.e4 (2017).
24. N. E. Rowland, M. J. Fregly, *Appetite* **11**, 143–178 (1988).
25. Y. Zhang *et al*., *Cell* **186**, 5751–5765.e16 (2023).
26. R. C. Bolles, *J. Comp. Physiol. Psychol.* **54**, 580–584 (1961).
27. A. V. Ferguson, R. J. Bicknell, M. A. Carew, W. T. Mason, *Neuroendocrinology* **66**, 409–415 (1997).
28. G. Yang *et al*., *Cell Discov.* **10**, 1 (2024).
29. I. R. Popescu *et al*., *Neurobiol. Aging* **98**, 88–98 (2021).
30. S. M. Mohr *et al*., *Nat. Commun.* **15**, 5803 (2024).
31. A. Jani *et al*., *Transplantation* **92**, 1215–1221 (2011).
32. E. M. Stricker, *Am. J. Physiol.* **217**, 98–105 (1969).
33. K. Schmidt-Nielsen, *Desert Animals: Physiological Problems of Heat and Water* (Oxford Univ. Press, 1964), pp. 9–10.
34. A. Bratincsák *et al*., *J. Comp. Neurol.* **505**, 443–458 (2007).
35. K. B. Hengen, M. Behan, H. V. Carey, M. V. Jones, S. M. Johnson, *Am. J. Physiol. Regul. Integr. Comp. Physiol.* **297**, R1028–R1036 (2009).
36. K. B. Hengen, T. M. Gomez, K. M. Stang, S. M. Johnson, M. Behan, *Am. J. Physiol. Regul. Integr. Comp. Physiol.* **300**, R272–R283 (2011).
37. L. J. Hoffstaetter *et al*., *Curr. Biol.* **28**, 2998–3004.e3 (2018).
38. R. Dai Pra, S. M. Mohr, D. K. Merriman, S. N. Bagriantsev, E. O. Gracheva, *Curr. Biol.* **32**, 1822–1828.e4 (2022).
39. M. J. McKinley, A. M. Allen, P. Burns, L. M. Colvill, B. J. Oldfield, *Clin. Exp. Pharmacol. Physiol. Suppl.* **25**, S61–S67 (1998).
40. B. J. Kinsman *et al*., *J. Neurosci.* **40**, 2069–2079 (2020).
41. T. Matsuda *et al*., *Nat. Neurosci.* **20**, 230–241 (2017).

ACKNOWLEDGMENTS

We thank S. Mohr and V. Feketa for assistance with transcriptome analysis and members of the Gracheva and Bagriantsev laboratories for their comments throughout the project. **Funding:** This work was funded by a Warren Alpert Distinguished Scholar Award (N.Y.F.), an Axle Tech International Endowed Professorship (D.K.M.), National Science Foundation grants IOS-2323133 (E.O.G.) and IOS-2015622 (E.O.G.), and National Institutes of Health grants R01NS126271 (E.O.G.) and R01NS132868 (S.N.B., E.O.G.). **Author contributions:** E.O.G. is the lead contact. Conceptualization: M.S.J., N.Y.F., S.N.B., E.O.G.; Methodology: M.S.J., N.Y.F., S.N.B., E.O.G.; Investigation: M.S.J., N.Y.F.; Formal analysis: M.S.J., N.Y.F.; Visualization: M.S.J.; Supervision: S.N.B., E.O.G.; Writing – original draft: M.S.J., S.N.B., E.O.G.; Writing – review and editing: M.S.J., N.Y.F., D.K.M., S.N.B., E.O.G. **Competing interests:** The authors declare that they have no competing interests. **Data and materials availability:** All data needed to evaluate the conclusions in this paper are present in the paper and/or the supplementary materials. RNA sequencing data have been deposited to the Gene Expression Omnibus under accession number GSE262723 and are publicly available.

SUPPLEMENTARY MATERIALS

science.org/doi/10.1126/science.adp8358
Materials and Methods
Figs. S1 to S4
Tables S1 and S2
References (*42*–*44*)
MDAR Reproducibility Checklist
Data S1

Submitted 14 April 2024; accepted 28 October 2024
10.1126/science.adp8358

Science
AAAS

Supplementary Materials for

Suppression of neurons in circumventricular organs enables months-long survival without water in thirteen-lined ground squirrels

Madeleine S. Junkins *et al.*

Corresponding authors: Sviatoslav N. Bagriantsev, slav.bagriantsev@yale.edu; Elena O. Gracheva, elena.gracheva@yale.edu

Science **386**, 1048 (2024)
DOI: 10.1126/science.adp8358

The PDF file includes:

Other Supplementary Material for this manuscript includes the following:

Materials and Methods

Animals

Squirrels were maintained in a colony at Yale University School of Medicine. All animal procedures were performed in compliance with the Office of Animal Research Support of Yale University (protocol 2024-11497). Thirteen-lined ground squirrels were implanted with an intrascapular temperature transponder (BMDS, LLC) and body temperature (T_b) was measured using a remote reader at least once per day. During the active season (Summer-Fall), animals were held in a vivarium with a room temperature of 18-20°C, a photoperiod of 12h:12h light:dark, and 40%-60% humidity. Squirrels were fed daily with dog food (Iams), sunflower seeds, superworms, and fresh vegetables, and given ad libitum access to water. During the hibernation season, animals who recently experienced hypothermic bouts were moved to a hibernaculum with 2-4°C room temperature, constant darkness, 40%–60% humidity, and no access to food or water.

Interbout arousal squirrels were defined as those whose T_b in the hibernaculum remained above 35°C for at least 1.5 hours following a torpor bout. Data from active squirrels was collected from June to October; data from interbout arousal squirrels was collected throughout the entire hibernation season, from August to March, since fluid homeostasis is essential throughout hibernation. In all cases, behavioral data and tissue samples were collected during the day. Prior to use, interbout arousal animals underwent a minimum of 2 and a maximum of 35 torpor bouts (mean = 11.66 days ± 1.28 SE), with a minimum of 1 and a maximum of 48 days in torpor since the previous interbout arousal (mean = 6.90 days ± 1.25 SE). Adolescent and adult males and females (aged 9 months – 3 years) were used for all studies and combined in analyses as fluid homeostasis is essential for the basic survival of both sexes. For all experiments, squirrels were selected at random. Sample size was determined from pilot experiments in our lab and previous work (*10*). Numbers of males and females for each experiment are reported in Table S1.

Serum Collection and ELISA

After squirrels were deeply anesthetized by isoflurane inhalation and prior to perfusion and brain collection, blood was collected by cardiac puncture and allowed to coagulate at room temperature for 30 min before spinning at 4°C for 15 min at 2000xg. Serum was removed and immediately stored at -80C until use.

Serum Angiotensin II and Serum Aldosterone were measured by ELISA according to the kit instructions (Enzo Life Sciences ADI-900-204 and ADI-900-173). All standards and samples

were run in duplicate. Optical density was read by a Spectramax 384 Plus plate reader (Molecular Devices) at the wavelength specific to the assay. Standard curves were fit with 4-parameter logistic regression in GraphPad Prism 10.0 (GraphPad Software).

Behavioral Experiments

Video monitoring occurred under a normal, 12h:12h light:dark cycle for active squirrels and under constant red light for interbout arousal squirrels so as not to interfere with hibernation. Videos were taken with Microsoft LifeCam Studio 1080p HD Webcam at the lowest frame rate (7.5 FPS) and written at 8X speed using custom MATLAB code. Raw video analysis for occurrence of drinking bouts was performed manually using VLC Media Player Version 3 with Jump to time (Previous frame) v3 extension. Total drinking duration, duration of each drinking bout, and the number of drinking bouts normalized by length of video recording was calculated using custom R script.

0.5 M NaCl and KCl

Drinking behavior was measured by continuous video monitoring over 6 h periods. Food and one bottle containing either water or 0.5 M NaCl were provided to active animals in the vivarium ad libitum. While interbout arousal animals normally do not have access to food or water in the hibernaculum, a bottle of either water, 0.5 M NaCl or 0.5 M KCl was provided to animals ad libitum during video recording experiments.

Drinking behavior during fasting

Drinking behavior was measured by continuous video monitoring in the vivarium. Animals were recorded for 24 h with food and water as a baseline. Then, food was removed and video monitoring was stopped. Following 24 h of food deprivation, video recording was resumed for an additional 24 h without food.

RNAScope

Squirrel *Agtr1* mRNA expression was detected with the RNAscope Multiplex Fluorescent Reagent Kit v2 Assay (Advanced Cell Diagnostics 323100) according to manufacturer's instructions. Squirrels were euthanized and transcardially perfused with ice-cold 4% paraformaldehyde in PBS, brain was dissected, fixed for 24 hr in 4% paraformaldehyde at 4°C on a rocker platform, sunk successively in 10, 20, and 30% sucrose solution in PBS at 4°C on a rocker platform, frozen in Tissue-Tek O.C.T. compound (Electron Microscopy Sciences 62550–01) and stored in the freezer at -80°C. Brain harvest was performed in strict RNAse free conditions.

14 μm sections of brain tissue were cut on a cryostat (Leica CM3500S). Sections containing the SFO were mounted on glass slides (Fisher Scientific 12-550-15), air dried for 1 hr at -20°C and stored at -80°C until use. On the day of the experiment, slides were washed with PBS, baked at 60°C for 30 min, post-fixed in 4% paraformaldehyde for 90 min at RT, dehydrated by successive incubation in 50, 70, and 100% (twice) ethanol for 5 min at RT, and air dried for 5 min. Sections were incubated with the RNAScope Squirrel *Agtr1* followed by incubation in TSA dilution reagent containing Fluorescein Green Opal 520 (Akoya Biosciences). Processed brain sections were imaged on a confocal microscope (Zeiss, LSM-780) with a 20X objective.

RNA Isolation and Sequencing

Bulk RNA Sequencing was performed as previously described (*30*). Squirrels were deeply anesthetized by isoflurane inhalation and subjected to intracardiac perfusion with ice-cold PBS. The brain was rapidly removed and a vibratome (Leica VT1200) was used to cut 300 μm coronal slices. Slices containing the SFO were identified by eye using the hippocampal commissure and third ventricle as landmarks. The SFO was manually dissected from the slices using 27G needles and placed immediately into RNA lysis buffer, and total RNA was then isolated using the Quick-RNA Microprep Kit (Zymo, R1050). RNA concentration and integrity number (RIN) were measured by NanoDrop and an Agilent 2100 Bioanalyzer (Agilent), respectively. RNA concentrations ranged from ~8.5 – 25.8 ng/μL (mean 15.63 ng/μL) and RIN values ranged from 6.8 – 9.1 (mean 8.29).

Library prep and sequencing were carried out at the Yale Center for Genome Analysis using the Illumina NovaSeq6000 in the 100 bp paired-end mode according to manufacturer's protocols.

The Yale Center for Research Computing cluster was used to process and analyze the sequencing data. Raw sequencing reads were filtered and trimmed to retain high-quality reads using Trimmomatic v0.39 with default parameters. Filtered high-quality reads from all samples were aligned to the *Ictidomys tridecemlineatus* reference genome using the STAR aligner v2.7.1a with default parameters. The SpeTri2.0 [GCA_000236235.1] reference genome and the gene annotation were obtained from the Broad Institute. The gene annotation was filtered to include only protein-coding genes. Aligned reads were counted by the featureCounts programs from the Subread package v2.2.0 with default parameters. Read counting was performed at the gene level, i.e., the final read count for each gene included all reads mapped to all exons of this gene. We

obtained a list of differential expression of genes by performing EdgeR v 3.30.3 (*42*) with the GLM approach and quasi-likelihood F-test, and using a significance value of FDR <0.05. Normalized read counts were obtained by normalizing raw read counts to effective library sizes of each sample and expressed as counts per million of total reads in a library (CPM).

RNA sequencing data are deposited to the Gene Expression Omnibus, accession number GSE262723 (Supplementary Data S1).

Fluorescent Angiotensin II Binding

Squirrels were anesthetized with isoflurane and injected via the tail artery with either Angiotensin II, TAMRA-labeled (AnaSpec AS-61181) or biocytin-TMR (ThermoFisher, T12921) at 1.5 µL/g body weight of 1 mg/mL solution prepared in DPBS with $Ca2^{+}$ and $Mg2^{+}$. Dye was allowed to circulate for 20 minutes while squirrels remained under anesthesia, until perfusion and tissue collection as described above (see RNAScope). Brains and livers were sectioned on a Leica cryostat (Leica CM3500S) at 40 µm and brain sections containing OVLT and SFO were saved for analysis. Sections were rinsed with PBS, mounted on glass slides (Fisher Scientific 12-550-15), and dried for 30 min at 37°C prior to being coverslipped with Vectashield containing DAPI (Vector Laboratories H-1200).

Z-stack images of liver, SFO and OVLT were acquired on a confocal microscope (Zeiss, LSM-780) using ZEN Software. Maximum intensity projection images were used for quantification in FIJI. Fluorescence intensity for the red channel was measured within ROIs manually drawn over SFO or OVLT, or the entire field of view for liver. Brain tracer fluorescence intensity was normalized to mean liver tracer fluorescence intensity from images with standardized acquisition settings.

Ratiometric Live-Cell Calcium Imaging

Primary thirst neurons were isolated according to published protocols (*43, 44*) with modifications. Squirrels were euthanized by isoflurane inhalation overdose followed by cardiac perfusion with Brain Perfusion Solution (containing in mM: 196 sucrose, 2.5 KCl, 28 $NaHCO_3$, 1.25 NaH_2PO_4, 7 Glucose, 1 Sodium Ascorbate, 0.5 $CaCl_2$, 7 $MgCl_2$, 3 Sodium Pyruvate, oxygenated with 95% O2/5% CO2, 300 mOsm, pH 7.4). The brain was dissected and brain slices were cut on a vibratome (VT1200, Leica Biosystems Inc, Buffalo Grove, IL). A brain slice containing either SFO or OVLT was identified and collected, and the region of interest was

manually dissected using 27G needles. Since the SFO is quite small, SFOs from 2-3 animals in the same state were pooled and digested together.

Tissue was digested in Hibernate A medium with 50 mM glucose and 280 mOsm (BrainBits) supplemented with 1 mM lactic acid (Sigma L1750) 0.5 mM GlutaMAX (ThermoFisher 35050061) and 2% B27 minus insulin (ThermoFisher A1895601) containing 20 U/ml papain (Worthington Biochemical LS003124) in a shaking water bath at 34°C for 30 min. The digested tissue was dissociated by mechanical trituration through the tips of glass Pasteur pipettes with decreasing diameter, after which the cell suspension was centrifuged over a layer of 8% bovine serum albumin (A9418-5G, Sigma). Dissociated neurons were resuspended in Neurobasal-A medium (ThermoFisher A2477501) adjusted to 2.5 mM glucose 280 mOsm and supplemented with 1 mM lactic acid, 0.5 mM GlutaMAX and 2% B27 minus insulin. Neurons were plated on poly-D-lysine/laminin-coated glass coverslips (Neuvitro, GG-12-Laminin) and cultured in an incubator at 34°C in 5% CO2. Neurons were loaded with 10 mM Fura 2-AM (ThermoFisher F1201) and 0.02% Pluronic F-127 (ThermoFisher P3000MP) in Ringer (in mM: 121 NaCl, 4.7 KCl, 2.5 D-glucose, 5 $NaHCO_3$, 2 $CaCl_2$, 0.1 $MgCl_2$, 1.2 $MgSO_4$, 0.97 KH_2PO_4, 0.23 K_2HPO_4, 25 HEPES, 290 mOsm, pH 7.4) for 30 min at 34°C and washed three times with Ringer.

Live-cell ratiometric calcium imaging was performed using the Axio-Observer Z1 inverted microscope (Carl Zeiss Inc) equipped with the Orca-Flash4.0 camera (Hamamatsu) using Meta-Fluor software v7.8.2.0 (Molecular Devices). Fluorescent images at 340 and 380 nm excitation were obtained with 10x objective every 1 s. Cells were continuously perfused with Ringer at a flow rate of ~5 ml/min. After obtaining baseline values at room temperature for 50 s, 10 nM Angiotensin II (Sigma Aldrich 05-23-0101) in Ringer was perfused at the same flow rate for 150 s, followed by 100s of washout with Ringer. At the end of the recording, cells were perfused with High K^+ Solution (in mM: 10 NaCl, 115.7 KCl, 2.5 D-glucose, 5 $NaHCO_3$, 2 $CaCl_2$, 0.1 $MgCl_2$, 1.2 $MgSO_4$, 0.97 KH_2PO_4, 0.23 K_2HPO_4, 25 HEPES, 290 mOsm, pH 7.4) to identify functional neurons.

Fluorescent images were processed offline. Regions of interest over imaged cells were created using MetaFluor software and manually revised as needed. A threshold was applied to the 340nm-excitation image to exclude regions not containing cells from calculations. The average 340/380 nm excitation ratio values over each region of interest were processed in Microsoft Excel

using a custom macro. Only cells passing the following criteria were included: average baseline (defined as the first 50 s of the recording) F ratio was below 0.8 fluorescence ratio units (non-normalized), the High K^+ response amplitude was above 1.35 units (after normalization to the baseline). The peak amplitudes of the responses to angiotensin II and High K^+ were determined using custom R script as the highest normalized fluorescence value. A neuron was defined as an angiotensin II responder if the amplitude of the response was greater than 1.13 fluorescence ratio units. These exclusion criteria were determined following data exploration from pilot experiments.

Immunohistochemistry (IHC)

Brains for IHC were harvested as above (see RNAScope). Coronal brain sections were cut on the cryostat at a thickness of 40 μm and mounted in parallel series on microscope slides and stored at -80 °C until further use.

Slides containing the SFO or OVLT were dried for 30 min in a 37°C incubator. The slides were washed three times with PBS for 10 min each. Three antigen retrieval steps were performed (*5*): 10 min in 1% H_2O_2 and 1% NaOH in PBS, 10 min in 0.3% glycine in PBS, and 10 min in 0.03% SDS in PBS. Slides were blocked with 5% Normal Goat Serum (NGS; Abcam AB138478) in 0.5% PBS-Tween20 (PBST) for 1 h at room temperature. Slides were then incubated for 48 h at 4°C with rabbit anti-nNOS (1:500 dilution, Abcam ab5586, RRID:AB_304965) and mouse anti-c-FOS (1:500 dilution, Santa Cruz sc-271243, RRID:AB_10610067) in 2% NGS in 0.1% PBST. Primary antibodies were refreshed after 24 h. After 48 h, the slides were washed with 0.1% PBST. Slides were then incubated with Goat anti-rabbit Alexa Fluor 555 (1:1000) and Goat anti-mouse Alexa Fluor 488 (1:400) in 0.1% PBST for 2 h at room temperature. The slides were washed with 0.1% PBST and rinsed with 1x PBS. Slides were mounted with Vectashield containing DAPI (Vector Laboratories H-1200) and imaged on a Zeiss LSM 900 Airyscan 2 with Axio Observer Microscope, Axiocam 705 Camera, and Zeiss Zen 3.5 Blue Edition software.

For each animal, 5 confocal images (for SFO) or 8-10 images (for OVLT) were analyzed in ImageJ (FIJI Version 1.0). Briefly, maximum intensity projection confocal images were split into red and green channels, and an appropriate threshold was determined for each channel by comparing several images taken from different animals. The same red and green channel thresholds were applied to all images from all animals within the same IHC experiment. Once thresholded, the Cell Counter plugin was used to count c-FOS^+ neurons, $nNOS^+$ c-FOS^+ neurons,

and nNOS$^-$ c-FOS$^+$ neurons. Counting was done under blinded conditions: all images were reassigned with random ID numbers during counting.

3 M NaCl Injection

Active and interbout arousal animals were immobilized with decapicones, weighed, and injected with intraperitoneally with 4.5 μL of 3 M NaCl per gram body weight. Squirrels were allowed to remain in a cage without water for 45 minutes prior to perfusion. For this experiment, serum was collected as described above and used for osmolality measurement on an OsmoTECH Osmometer (Advanced Instruments).

Patch-clamp Electrophysiology

Squirrels were deeply anesthetized with isoflurane and immediately decapitated. The brain was rapidly dissected and immersed in Hibernate A medium (50 mM glucose, 280 mOsm, BrainBits) supplemented with 1 mM lactic acid (Cat. #L1750, Sigma) 0.5 mM GlutaMAX (Cat. #35050061, ThermoFisher) and 2% B27 minus insulin (Cat. #A1895601, ThermoFisher). Brains were sliced with a coronal rodent brain matrix (Electron Microscopy Sciences), and SFOs from two animals were collected and pooled. Tissue digestion and trituration proceeded in a manner similar to the protocol described above (see Ratiometric Live-Cell Calcium Imaging), with the exception that after plating, neurons were rinsed in Neurobasal and allowed to incubate overnight for 18-24 hours before recording.

Data were acquired on a Zeiss Axio-Examiner with an Orca flash 4.0 camera (Hamamatsu) and an Axopatch 200-B amplifier/Digidata 1440 digitizer (Molecular Devices). Recordings were acquired using pCLAMP software (Molecular Devices) sampled at 20-50 kHz and low-pass filtered at 2–10 kHz. Experiments were carried out at a room temperature of 22–25°C. Coverslips were placed into the recording chamber with Ringer (in mM: 121 NaCl, 4.7 KCl, 2.5 D-glucose, 5 $NaHCO_3$, 2 $CaCl_2$, 0.1 $MgCl_2$, 1.2 $MgSO_4$, 0.97 KH_2PO_4, 0.23 K_2HPO_4, 25 HEPES, osmolarity adjusted to 300 mOsm with NaCl, pH 7.4) at RT. The internal pipette solution consisted of (in mM): 135 K-gluconate, 5 KCl, 5 EGTA, 0.5 $CaCl_2$, 2 $MgCl_2$, 5 HEPES, 5 Na_2ATP, 0.5 Na_2GTP (adjusted to pH 7.403 with KOH and some HCl, osmolarity adjusted to 292 mOsm with 9 mM glucose). Patch pipettes of borosilicate glass with an outer diameter of 1.5 mm (Warner Instruments no. G150F-3) were pulled and polished to a tip resistance of 4–10 MΩ using a P-1000 puller (Sutter Instruments) and CPM-2 (ALA Scientific Instruments) microforge. Experiments were not corrected for liquid junction potential. Immediately after whole-cell recording was

established, a brief ~10 second protocol was run in voltage clamp to measure input resistance. Resting membrane potential was then measured in I = 0 mode, before switching to current clamp. Cells that were more depolarized than -40 mV at rest were rejected, based on predetermined exclusion criteria. Action potential firing was often spontaneous, but if not, it could be elicited by applying a depolarizing holding current between 3-10 pA.

An image of each neuron was recorded, and neuron diameter was measured in ImageJ (NIH) as the average of the long and short axes. All further analysis was done in Clampfit (pCLAMP, Molecular Devices). Input resistance was calculated by recording current changes by a voltage injection of -5 mV. Peak amplitude was measured from the baseline to the maximum amplitude of the action potential. Maximal hyperpolarization was defined as the point furthest in amplitude from the peak. Rise slope and rise time were measured from 20%–80% of the peak maximum. Half-width was defined as the time between the points to the left and right of the peak representing 50% of the peak amplitude.

For the GABA experiment in Figure 4Q, a 10 μM solution of GABA (Cat. #A2129, Sigma) was prepared in Ringer. During each recording, a neuron was perfused, under a constant flow rate, with Ringer for 60 seconds, followed by 10 μM GABA for 50 seconds, followed by washout with Ringer for 2 minutes.

Statistical Analysis

Statistical analyses were performed in GraphPad Prism 10.0 (GraphPad Software) and R (R version 4.3.2). Tests were chosen based on normality, data distribution and experimental design, and detailed accordingly in the figure legends. Sample sizes for each experiment are noted in figure legends. Numbers above data in all figures denote p values.

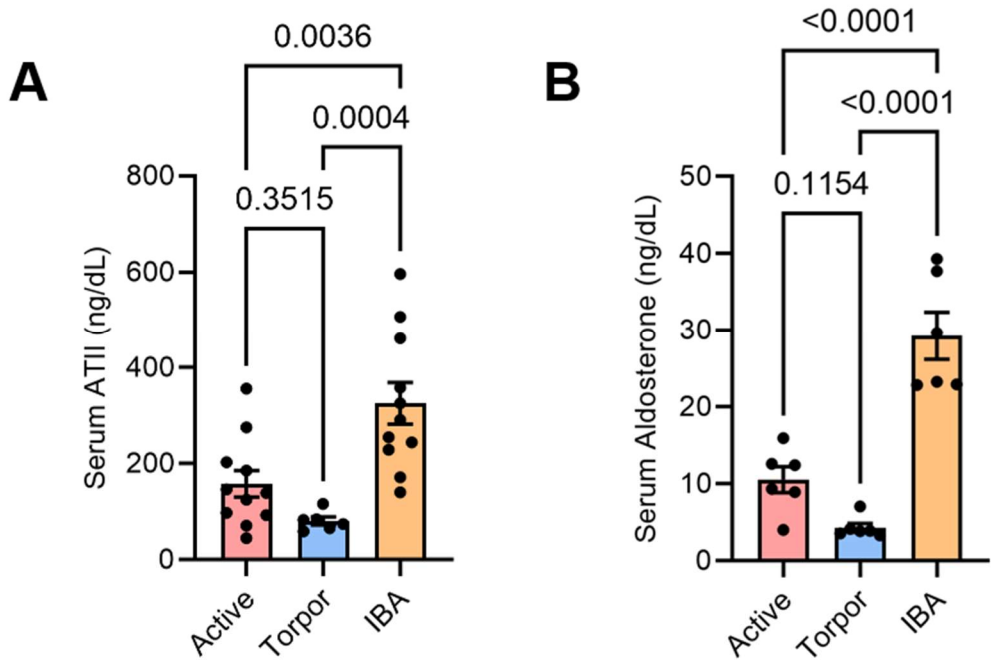

Fig. S1. Angiotensin II and aldosterone across hibernation states.

(**A**) Serum angiotensin II measurements from active (n = 11), torpid (n = 6) and interbout arousal (n = 11) squirrels. One-way ANOVA: a significant main effect of state ($F_{2,25} = 11.78$, $p = 0.0002$). Tukey's multiple comparisons test. Active and interbout arousal data from Figure 1A.

(**B**) Serum aldosterone measurements from active (n = 6), torpid (n = 6) and interbout arousal (n = 6) squirrels. One-way ANOVA: a significant main effect of state ($F_{2,15} = 39.84$, $p < 0.0001$). Tukey's multiple comparisons test. Active and interbout arousal data from Figure 1B.

Dots represent data from individual animals (mean ± SE). Numbers above data denote p values. IBA, interbout arousal.

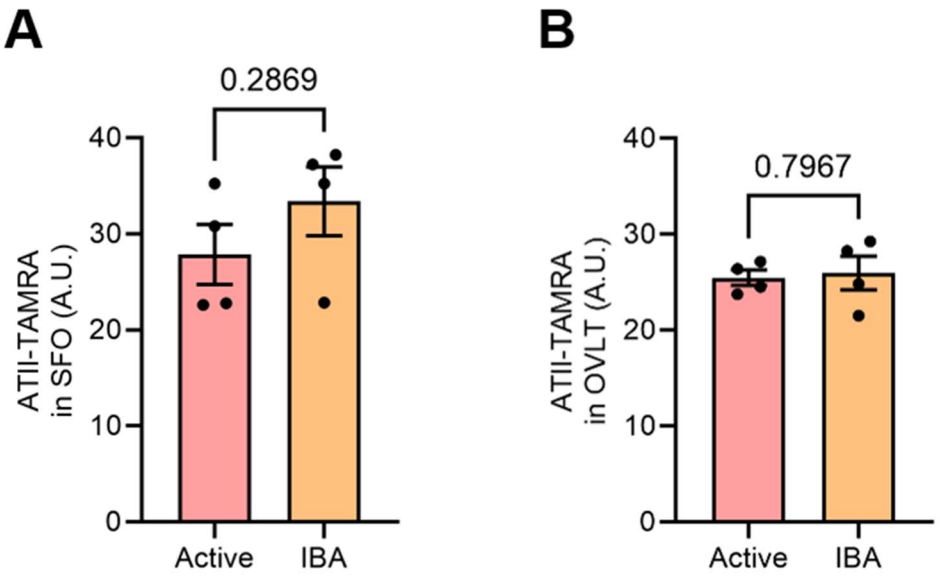

Fig. S2. Quantification of raw ATII-TAMRA levels in SFO and OVLT.

(**A**) Quantification of ATII-TAMRA dye intensity in SFO from active (n = 4) and interbout arousal (n = 4) squirrels without normalization to liver intensity.

(**B**) Quantification of ATII-TAMRA dye intensity in OVLT from active (n = 4) and interbout arousal (n = 4) squirrels without normalization to liver intensity.

Dots represent an average of ≥ 3 images from individual animals (mean ± SE). Numbers above data denote p values. IBA, interbout arousal.

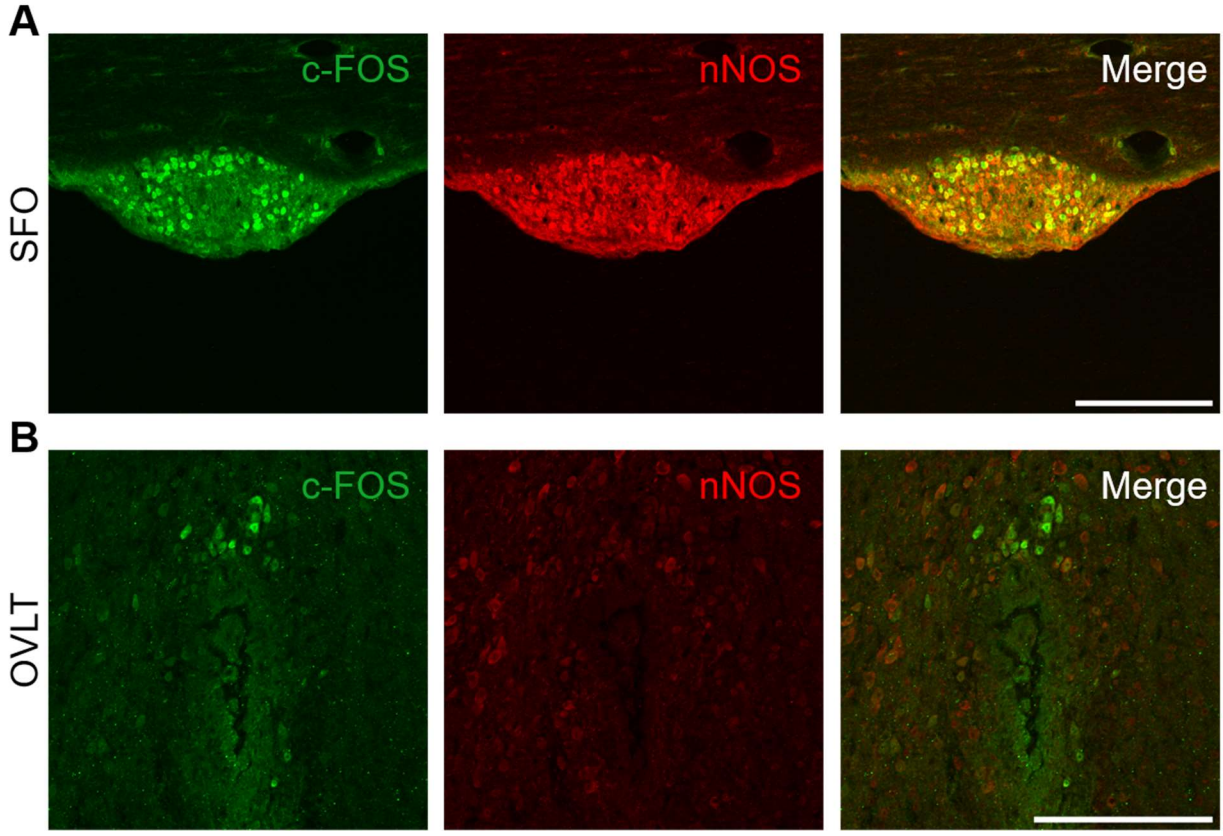

Fig. S3. Co-immunostaining of c-FOS with nNOS in SFO and OVLT of active untreated squirrels.

(**A**) Representative c-FOS (green), nNOS (red) and co-stained images of a section of SFO from an active, untreated squirrel (same as Figure 3A, left panel).

(**B**) Representative c-FOS (green), nNOS (red) and co-stained images of a section of OVLT from an active, untreated squirrel (same as Figure 3E, left panel).

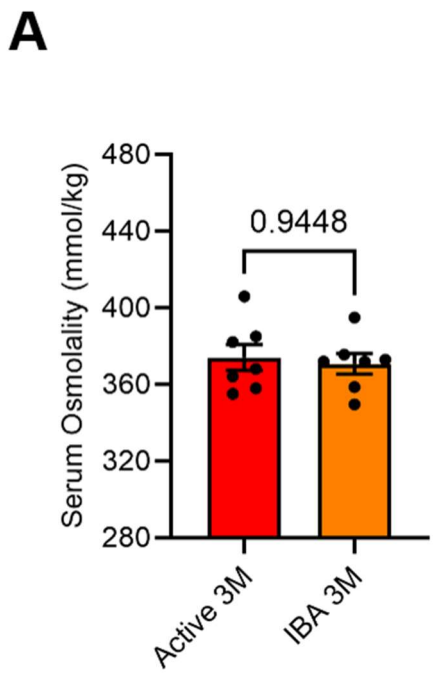

Fig. S4. Effect of 3 M NaCl i.p. treatment on serum osmolality in active and interbout arousal squirrels.

(**A**) Serum osmolality of active (n = 7) and interbout arousal (n = 7) squirrels 45 minutes after treatment with 4.5 µL/g of 3 M NaCl i.p. Dots represent individual animals (mean ± SE). Numbers above data denote p values. IBA, interbout arousal.

Table S1. The number of females (F) and males (M) in each group for each experiment.

EXPERIMENT	ACTIVE	INTERBOUT AROUSAL
SERUM ANGIOTENSIN II	2F 9M	4F 7M
SERUM ALDOSTERONE	1F 5M	3F 3M
0.5 M NACL DRINKING BEHAVIOR	4F 7M	9F 9M
0.5 M KCL DRINKING BEHAVIOR	-	2F 4M
FOOD DEPRIVED DRINKING BEHAVIOR	3F 5M	-
RNA-SEQ	3F 2M	1F 4M
ATII-TAMRA	2F 2M	3F 1M
CALCIUM IMAGING SFO	5F 1M	7F 4M
CALCIUM IMAGING OVLT	2F 2M	1F 3M
IHC SFO NT	1F 2M	2F 1M
IHC OVLT NT	1F 2M	2F 1M
IHC SFO 3M	1F 2M	1F 2M
IHC OVLT 3M	2F 1M	0F 3M
ELECTROPHYSIOLOGY	7F 3M	3F 3M

Table S2. (separate file)
The source data used to create all figures.

Data S1. (separate file)
Bulk RNA sequencing data of the subfornical organ of active and interbout arousal squirrels. Data deposited to the Gene Expression Omnibus, accession number GSE262723.

References and Notes

1. W. E. Allen, L. A. DeNardo, M. Z. Chen, C. D. Liu, K. M. Loh, L. E. Fenno, C. Ramakrishnan, K. Deisseroth, L. Luo, Thirst-associated preoptic neurons encode an aversive motivational drive. *Science* **357**, 1149–1155 (2017). doi:10.1126/science.aan6747 Medline

2. J. T. Fitzsimons, Angiotensin, thirst, and sodium appetite. *Physiol. Rev.* **78**, 583–686 (1998). doi:10.1152/physrev.1998.78.3.583 Medline

3. Y. Oka, M. Ye, C. S. Zuker, Thirst driving and suppressing signals encoded by distinct neural populations in the brain. *Nature* **520**, 349–352 (2015). doi:10.1038/nature14108 Medline

4. V. Augustine, S. K. Gokce, S. Lee, B. Wang, T. J. Davidson, F. Reimann, F. Gribble, K. Deisseroth, C. Lois, Y. Oka, Hierarchical neural architecture underlying thirst regulation. *Nature* **555**, 204–209 (2018). doi:10.1038/nature25488 Medline

5. C. A. Zimmerman, Y. C. Lin, D. E. Leib, L. Guo, E. L. Huey, G. E. Daly, Y. Chen, Z. A. Knight, Thirst neurons anticipate the homeostatic consequences of eating and drinking. *Nature* **537**, 680–684 (2016). doi:10.1038/nature18950 Medline

6. K. Schmidt-Nielsen, B. Schmidt-Nielsen, Water metabolism of desert mammals 1. *Physiol. Rev.* **32**, 135–166 (1952). doi:10.1152/physrev.1952.32.2.135 Medline

7. D. E. Leib, C. A. Zimmerman, Z. A. Knight, Thirst. *Curr. Biol.* **26**, R1260–R1265 (2016). doi:10.1016/j.cub.2016.11.019 Medline

8. V. Augustine, S. Lee, Y. Oka, Neural control and modulation of thirst, sodium appetite, and hunger. *Cell* **180**, 25–32 (2020). doi:10.1016/j.cell.2019.11.040 Medline

9. M. S. Junkins, S. N. Bagriantsev, E. O. Gracheva, Towards understanding the neural origins of hibernation. *J. Exp. Biol.* **225**, jeb229542 (2022). doi:10.1242/jeb.229542 Medline

10. N. Y. Feng, M. S. Junkins, D. K. Merriman, S. N. Bagriantsev, E. O. Gracheva, Osmolyte depletion and thirst suppression allow hibernators to survive for months without water. *Curr. Biol.* **29**, 3053–3058.e3 (2019). doi:10.1016/j.cub.2019.07.038 Medline

11. S. M. Mohr, S. N. Bagriantsev, E. O. Gracheva, Cellular, molecular, and physiological adaptations of hibernation: The solution to environmental challenges. *Annu. Rev. Cell Dev. Biol.* **36**, 315–338 (2020). doi:10.1146/annurev-cellbio-012820-095945 Medline

12. M. S. Junkins, N. Y. Feng, L. A. Murphy, G. Curtis, D. K. Merriman, S. N. Bagriantsev, E. O. Gracheva, Neural control of fluid homeostasis is engaged below 10°C in hibernation. *Curr. Biol.* **34**, 923–930.e5 (2024). doi:10.1016/j.cub.2024.01.035 Medline

13. B. Kisser, H. T. Goodwin, Hibernation and overwinter body temperatures in free-ranging thirteen-lined ground squirrels, *Ictidomys tridecemlineatus*. *Am. Midl. Nat.* **167**, 396–409 (2012). doi:10.1674/0003-0031-167.2.396

14. A. T. Rasmussen, Theories of hibernation. *Am. Nat.* **50**, 609–625 (1916). doi:10.1086/279571

15. A. H. Pool, T. Wang, D. A. Stafford, R. K. Chance, S. Lee, J. Ngai, Y. Oka, The cellular basis of distinct thirst modalities. *Nature* **588**, 112–117 (2020). doi:10.1038/s41586-020-2821-8 Medline

16. J. M. Resch, H. Fenselau, J. C. Madara, C. Wu, J. N. Campbell, A. Lyubetskaya, B. A. Dawes, L. T. Tsai, M. M. Li, Y. Livneh, Q. Ke, P. M. Kang, G. Fejes-Tóth, A. Náray-Fejes-Tóth, J. C. Geerling, B. B. Lowell, Aldosterone-sensing neurons in the NTS exhibit state-dependent pacemaker activity and drive sodium appetite via synergy with

angiotensin II signaling. *Neuron* **96**, 190–206.e7 (2017). doi:10.1016/j.neuron.2017.09.014 Medline

17. A. Spät, L. Hunyady, Control of aldosterone secretion: A model for convergence in cellular signaling pathways. *Physiol. Rev.* **84**, 489–539 (2004). doi:10.1152/physrev.00030.2003 Medline

18. J. C. Geerling, A. D. Loewy, Central regulation of sodium appetite. *Exp. Physiol.* **93**, 177–209 (2008). doi:10.1113/expphysiol.2007.039891 Medline

19. B. C. Jarvie, R. D. Palmiter, HSD2 neurons in the hindbrain drive sodium appetite. *Nat. Neurosci.* **20**, 167–169 (2017). doi:10.1038/nn.4451 Medline

20. A. I. Hicks, S. Kobrinsky, S. Zhou, J. Yang, M. Prager-Khoutorsky, Anatomical organization of the rat subfornical organ. *Front. Cell. Neurosci.* **15**, 691711 (2021). doi:10.3389/fncel.2021.691711 Medline

21. M. Prager-Khoutorsky, C. W. Bourque, Anatomical organization of the rat organum vasculosum laminae terminalis. *Am. J. Physiol. Regul. Integr. Comp. Physiol.* **309**, R324–R337 (2015). doi:10.1152/ajpregu.00134.2015 Medline

22. C. W. Bourque, Central mechanisms of osmosensation and systemic osmoregulation. *Nat. Rev. Neurosci.* **9**, 519–531 (2008). doi:10.1038/nrn2400 Medline

23. D. E. Leib, C. A. Zimmerman, A. Poormoghaddam, E. L. Huey, J. S. Ahn, Y. C. Lin, C. L. Tan, Y. Chen, Z. A. Knight, The forebrain thirst circuit drives drinking through negative reinforcement. *Neuron* **96**, 1272–1281.e4 (2017). doi:10.1016/j.neuron.2017.11.041 Medline

24. N. E. Rowland, M. J. Fregly, Sodium appetite: Species and strain differences and role of renin-angiotensin-aldosterone system. *Appetite* **11**, 143–178 (1988). doi:10.1016/S0195-6663(88)80001-1 Medline

25. Y. Zhang, A. H. Pool, T. Wang, L. Liu, E. Kang, B. Zhang, L. Ding, K. Frieda, R. Palmiter, Y. Oka, Parallel neural pathways control sodium consumption and taste valence. *Cell* **186**, 5751–5765.e16 (2023). doi:10.1016/j.cell.2023.10.020 Medline

26. R. C. Bolles, The interaction of hunger and thirst in the rat. *J. Comp. Physiol. Psychol.* **54**, 580–584 (1961). doi:10.1037/h0044595 Medline

27. A. V. Ferguson, R. J. Bicknell, M. A. Carew, W. T. Mason, Dissociated adult rat subfornical organ neurons maintain membrane properties and angiotensin responsiveness for up to 6 days. *Neuroendocrinology* **66**, 409–415 (1997). doi:10.1159/000127266 Medline

28. G. Yang, M. Jia, G. Li, Y. Y. Zang, Y. Y. Chen, Y. Y. Wang, S. Y. Zhan, S. X. Peng, G. Wan, W. Li, J. J. Yang, Y. S. Shi, TMEM63B channel is the osmosensor required for thirst drive of interoceptive neurons. *Cell Discov.* **10**, 1 (2024). doi:10.1038/s41421-023-00628-x Medline

29. I. R. Popescu, K. Q. Le, A. L. Ducote, J. E. Li, A. E. Leland, R. Mostany, Increased intrinsic excitability and decreased synaptic inhibition in aged somatosensory cortex pyramidal neurons. *Neurobiol. Aging* **98**, 88–98 (2021). doi:10.1016/j.neurobiolaging.2020.10.007 Medline

30. S. M. Mohr, R. Dai Pra, M. P. Platt, V. V. Feketa, M. Shanabrough, L. Varela, A. Kristant, H. Cao, D. K. Merriman, T. L. Horvath, S. N. Bagriantsev, E. O. Gracheva, Hypothalamic hormone deficiency enables physiological anorexia in ground squirrels during hibernation. *Nat. Commun.* **15**, 5803 (2024). doi:10.1038/s41467-024-49996-2 Medline

31. A. Jani, E. Epperson, J. Martin, A. Pacic, D. Ljubanovic, S. L. Martin, C. L. Edelstein, Renal protection from prolonged cold ischemia and warm reperfusion in hibernating squirrels. *Transplantation* **92**, 1215–1221 (2011). doi:10.1097/TP.0b013e3182366401 Medline

32. E. M. Stricker, Osmoregulation and volume regulation in rats: Inhibition of hypovolemic thirst by water. *Am. J. Physiol.* **217**, 98–105 (1969). doi:10.1152/ajplegacy.1969.217.1.98 Medline

33. K. Schmidt-Nielsen, *Desert Animals: Physiological Problems of Heat and Water* (Oxford Univ. Press, 1964), pp. 9–10.

34. A. Bratincsák, D. McMullen, S. Miyake, Z. E. Tóth, J. M. Hallenbeck, M. Palkovits, Spatial and temporal activation of brain regions in hibernation: *c-fos* expression during the hibernation bout in thirteen-lined ground squirrel. *J. Comp. Neurol.* **505**, 443–458 (2007). doi:10.1002/cne.21507 Medline

35. K. B. Hengen, M. Behan, H. V. Carey, M. V. Jones, S. M. Johnson, Hibernation induces pentobarbital insensitivity in medulla but not cortex. *Am. J. Physiol. Regul. Integr. Comp. Physiol.* **297**, R1028–R1036 (2009). doi:10.1152/ajpregu.00239.2009 Medline

36. K. B. Hengen, T. M. Gomez, K. M. Stang, S. M. Johnson, M. Behan, Changes in ventral respiratory column $GABA_aR$ ε- and δ-subunits during hibernation mediate resistance to depression by EtOH and pentobarbital. *Am. J. Physiol. Regul. Integr. Comp. Physiol.* **300**, R272–R283 (2011). doi:10.1152/ajpregu.00607.2010 Medline

37. L. J. Hoffstaetter, M. Mastrotto, D. K. Merriman, S. D. Dib-Hajj, S. G. Waxman, S. N. Bagriantsev, E. O. Gracheva, Somatosensory neurons enter a state of altered excitability during hibernation. *Curr. Biol.* **28**, 2998–3004.e3 (2018). doi:10.1016/j.cub.2018.07.020 Medline

38. R. Dai Pra, S. M. Mohr, D. K. Merriman, S. N. Bagriantsev, E. O. Gracheva, Ground squirrels initiate sexual maturation during hibernation. *Curr. Biol.* **32**, 1822–1828.e4 (2022). doi:10.1016/j.cub.2022.02.032 Medline

39. M. J. McKinley, A. M. Allen, P. Burns, L. M. Colvill, B. J. Oldfield, Interaction of circulating hormones with the brain: The roles of the subfornical organ and the organum vasculosum of the lamina terminalis. *Clin. Exp. Pharmacol. Physiol. Suppl.* **25**, S61–S67 (1998). doi:10.1111/j.1440-1681.1998.tb02303.x Medline

40. B. J. Kinsman, S. S. Simmonds, K. N. Browning, M. M. Wenner, W. B. Farquhar, S. D. Stocker, Integration of hypernatremia and angiotensin II by the organum vasculosum of the lamina terminalis regulates thirst. *J. Neurosci.* **40**, 2069–2079 (2020). doi:10.1523/JNEUROSCI.2208-19.2020 Medline

41. T. Matsuda, T. Y. Hiyama, F. Niimura, T. Matsusaka, A. Fukamizu, K. Kobayashi, K. Kobayashi, M. Noda, Distinct neural mechanisms for the control of thirst and salt appetite in the subfornical organ. *Nat. Neurosci.* **20**, 230–241 (2017). doi:10.1038/nn.4463 Medline

42. M. D. Robinson, D. J. McCarthy, G. K. Smyth, edgeR: A Bioconductor package for differential expression analysis of digital gene expression data. *Bioinformatics* **26**, 139–140 (2010). doi:10.1093/bioinformatics/btp616 Medline

43. V. V. Feketa, Y. A. Nikolaev, D. K. Merriman, S. N. Bagriantsev, E. O. Gracheva, CNGA3 acts as a cold sensor in hypothalamic neurons. *eLife* **9**, e55370 (2020). doi:10.7554/eLife.55370 Medline

44. R. P. Vazirani, X. Fioramonti, V. H. Routh, Membrane potential dye imaging of ventromedial hypothalamus neurons from adult mice to study glucose sensing. *J. Vis. Exp.* **2013**, 50861 (2013). doi:10.3791/50861-v Medline